AgriEngineering

Article

Prediction of Corn Leaf Nitrogen Content in a Tropical Region Using Vis-NIR-SWIR Spectroscopy

Ana Karla da Silva Oliveira, Rodnei Rizzo *, Carlos Augusto Alves Cardoso Silva, Natália Correr Ré, Matheus Luís Caron and Peterson Ricardo Fiorio

Graduate Program on Agricultural Systems Engineering, "Luiz de Queiroz" College of Agriculture, University of São Paulo, Piracicaba 13418900, SP, Brazil; anakarla95@usp.br (A.K.d.S.O.); carlosesalq@usp.br (C.A.A.C.S.); natalia.re@usp.br (N.C.R.); matheuscaron@usp.br (M.L.C.); fiorio@usp.br (P.R.F.)

* Correspondence: rodnei.rizzo@gmail.com

Abstract: Traditional techniques for measuring leaf nitrogen content (LNC) involve slow and laborious processes, and radiometric data have been used to assist in the nutritional analysis of plants. Therefore, this study aimed to evaluate the performance of LNC predictions in corn plants based on laboratory hyperspectral Vis-NIR-SWIR data. The treatments corresponded to 60, 120, 180, and 240 kg ha^{-1} of nitrogen, in addition to the control (0 kg ha^{-1}), and they were distributed using a randomized complete block design. At the laboratory, hyperspectral data of the leaves and LNC were obtained. The hyperspectral data were used in the calculation of different vegetation indices (VIs), which were applied in a predictive model—partial least squares regression (PLSR)—and the capacity of the prediction was assessed. The combination of bands and VIs generated a better prediction ($0.74 < R^2 < 0.87$; $1.00 <$ RMSE < 1.50 kg ha^{-1}) in comparison with the individual prediction by band ($0.69 < R^2 < 0.85$; $1.00 <$ RMSE < 1.77 kg ha^{-1}) and by VI ($0.55 < R^2 < 0.68$; $1.00 <$ RMSE < 1.78 kg ha^{-1}). Hyperspectral data offer a new opportunity to monitor the LNC in corn plants, especially in the region comprising the bands from 450 to 750 nm, since these were the bands that were most sensitive to the LNC.

Keywords: nutritional status; hyperspectral data; leaf nitrogen content

check for updates

Citation: Oliveira, A.K.d.S.; Rizzo, R.; Silva, C.A.A.C.; Ré, N.C.; Caron, M.L.; Fiorio, P.R. Prediction of Corn Leaf Nitrogen Content in a Tropical Region Using Vis-NIR-SWIR Spectroscopy. *AgriEngineering* **2024**, *6*, 4135–4153. https://doi.org/10.3390/agriengineering6040233

Academic Editors: Murali Krishna Gumma and Simone Pascuzzi

Received: 2 September 2024
Revised: 18 October 2024
Accepted: 28 October 2024
Published: 31 October 2024

1. Introduction

Corn (*Zea mays* L.) is one of the most important crops in the Brazilian agribusiness production chain. The growing demand for corn reinforces its potential not only as a food source, with a high relevance for livestock and agriculture, but also as an indispensable raw material in nutrition, health, the chemical industry, and bioenergy [1]. Furthermore, corn has an essential function in soil conservation and the sustainability of production systems due to the high amount of straw produced from corn, which, in turn, helps with protection, nutrient cycling, and increasing soil organic matter (SOM), in addition to its roots helping with soil decompression [2].

Among the main limiting factors in the development of corn plants, the nutritional supply stands out. The management of and recommendations for nitrogen (N) are complex, given the various chemical and biological reactions that influence it and its great dependence on edaphoclimatic conditions for absorption by the plant [3]. N monitoring and quantification are based on conventional approaches, including an analysis of plant tissues [4]. Analyzing the leaf nutrient content is one strategy for monitoring crops and adequately managing nitrogen-based fertilizers.

However, these methods are expensive, in addition to presenting limitations in large-scale applications due to the slow speed of data acquisition and the demand for a large number of samples [5]. Alternatively, hyperspectral remote sensing (RS), a technique described as an ally in the efficiency of agricultural production systems, has emerged as an agile, effective, and low-cost tool, and studies on the application of RS in the monitoring

of leaf nitrogen levels in crops have great significance [6–9]. The spectral reflectance of plants in the Vis-NIR-SWIR range provides important information on the N status of crops. Remote sensing indicators of N status are related to chlorophyll or N concentration, and hyperspectral data are usually obtained from crop leaves or the whole canopy. Some studies describe the significant relationship between the leaves/canopy and grain yield in cereal crops [10,11]. Photosynthesis is the primary determinant of the conversion of light into biomass and is one of the driving factors of crop yield, whether biomass or grain production [12]. Therefore, remote sensing indicators derived from the aerial structure of plants usually provide important information for crop monitoring, including an assessment of nutrient status.

In addition, the potential of VIs to estimate leaf N has been widely explored. VIs have applications in several crops, such as wheat [13], corn [14], sugarcane [15], and others [16], since indices are generally simple to calculate and can reduce the interference from other targets [17]. Nonetheless, hyperspectral data, due to their quantity, require robust techniques to be evaluated, such as partial least squares regression (PLSR). This method has been frequently applied to detect nutritional deficiencies, especially when hyperspectral data are used [7,18,19], because it is a statistical procedure that flexibly adjusts leaf spectra, measuring several characteristics with a high predictive performance [20,21].

Promising results have been obtained using PLSR for nutrient predictions (R^2 = 0.76 and RMSE = 0.11 g kg^{-1}) in sugarcane [22]; in rice, with the R^2 varying from 0.68 to 0.87 and NRMSE varying from 10 to 29% [23]; in soybeans (R^2 = 0.80) [24]; and in pine trees, with an R^2 = 0.62 [25]. Reports on nitrogen predictions in corn leaves have also presented promising results, with R^2 ranging from 0.6 to 0.9. Zhang et al. [26] developed an NIR device to retrieve the spectra from corn crops and predict the average nitrogen content in fresh leaves. In this case, the models' performance corresponded to an R^2 = 0.75 and an RMSE = 0.26 g. Silva et al. [27] evaluated the effect of different abiotic stress treatments on maize and sorghum leaves. Vis-NIR-SWIR and mid-infrared (MIR) spectra were used to calibrate the PLSR models, and the results were an R^2 between 0.77 and 0.93. Xie et al. [28] found that the best spectral region for N predictions in corn leaves was 350–1000 nm, and they were able to calibrate models with an R^2 and RMSE of 0.65 and 0.26, respectively. Ge at al. [23] predicted the nitrogen levels of leaves with different water content levels and indicated that the models calibrated with Vis-NIR-SWIR spectra had a good performance (R^2 = 0.86 and RPD = 2.64). Nevertheless, these studies suggest that further investigations are needed regarding the nutritional analysis; given the complexity inherent in nitrogen dynamics in soil and crops, robust and reliable techniques regarding the leaf nitrogen content (LNC) require more in-depth investigations, with the aim of improving the understanding of the information offered by the spectral response.

Therefore, this study aimed to evaluate the performance of LNC predictions in corn plants through the partial least squares regression algorithm. While many studies have evaluated the potential of Vis-NIR-SWIR spectroscopy to predict leaf nitrogen in corn fields in North America and Europe, very few have tested this method under tropical conditions. Due to the differences in the soil, climate, and plant cultivars, it is extremely important to evaluate the method's potential under different environmental conditions. Thus, this research aimed to obtain insights into N quantification using spectroradiometry, as well as discuss the methodological limitations that still need to be overcome.

2. Materials and Methods

2.1. Experiment Description

This experiment was performed at the "Luiz de Queiroz" College of Agriculture (ESALQ/USP) in the municipality of Piracicaba, at the geographic coordinates 22°41′54″ S, 47°38′34″ W, and an altitude of 540 m (Figure 1). The soil in the region is classified as Nitisol according to the World Reference Base [29], presenting a high base saturation and clay content. According to the Köppen classification, the local climate is of the Cwa type, humid subtropical, with dry winters and rainy summers, an average rainfall of 1247 mm year^{-1},

an average temperature in the hottest month of 22 °C and an average temperature in the coldest month of 18 °C, an average relative humidity of 74%, and an average wind speed of 2.2 m s^{-1} [30].

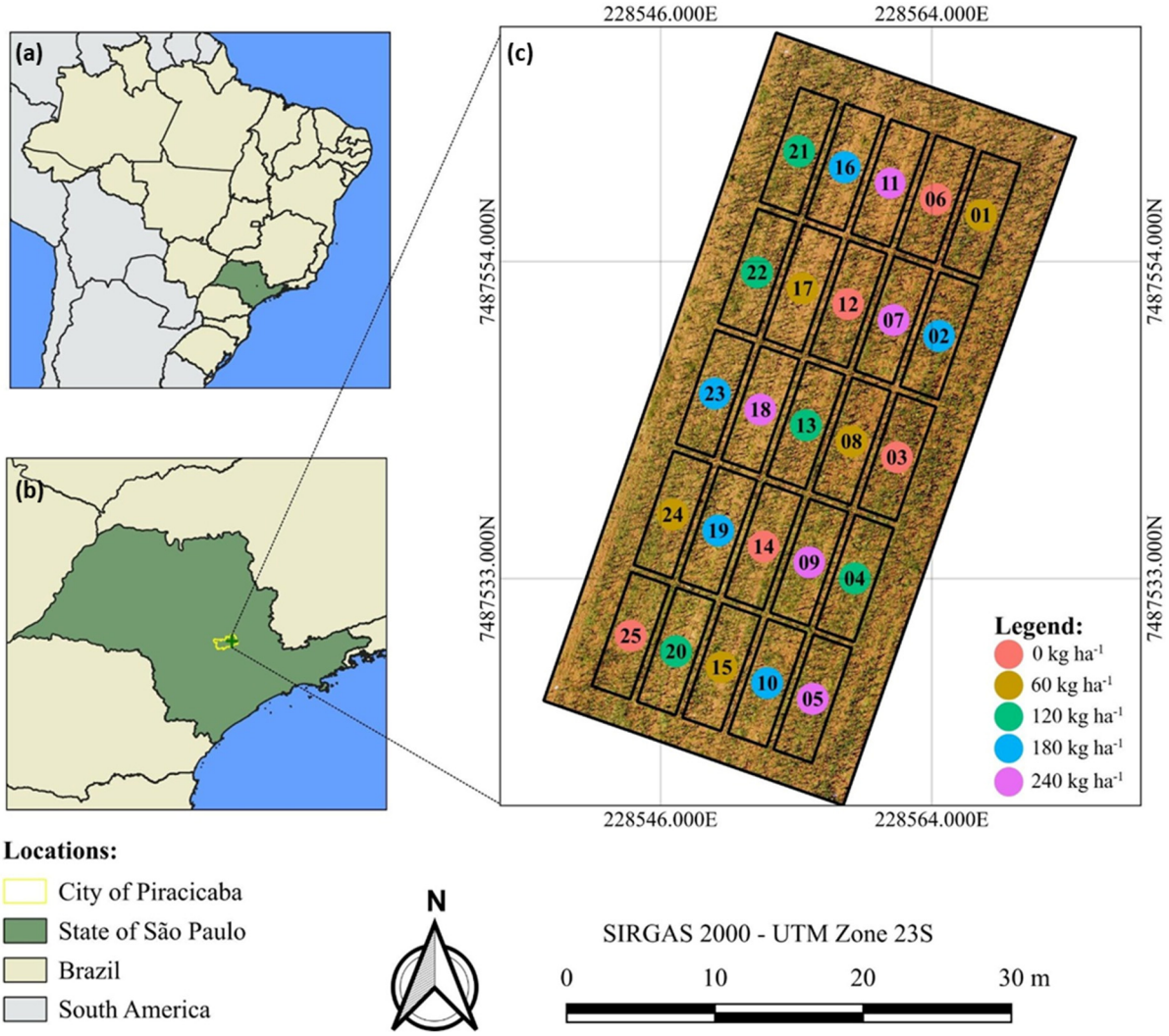

Figure 1. Site location in Brazil (**a**) and in the State of São Paulo (**b**). Experimental design and nitrogen doses (**c**).

Sowing occurred on 11 December 2021, and the corn cultivar used was SHS7939, a hybrid considered early with a high productivity. This cultivar is grown throughout Brazil, both in the summer and in the off-season. It is used in the production of grains, whole plant silage, and wet grain silage.

2.1.1. Description of Fertilization and Design

The treatments corresponded to doses of 60, 120, 180, and 240 kg of nitrogen per ha^{-1}, in addition to the control (without nitrogen application), using urea as the fertilizer. The experimental design adopted was a randomized complete block design (RCBD) with five treatments and five replications, totaling 25 plots. Each plot consisted of 6 corn rows (4 central rows and 2 border rows), with dimensions of 8 × 2.7 m (Figure 1). Fertilization was conducted in a fractional way, with the application of 30 kg ha^{-1} of fertilizer at sowing and the remainder divided into two equal parts distributed at vegetative growth stages 3 (V3) and 5 (V5) (Table 1).

Table 1. Fertilization distribution.

Treatments	Doses	Seeding	V3	V5
		---- Nitrogen in kg ha^{-1} -----		
T1	0	0	0	0
T2	60	30	15	15
T3	120	30	45	45
T4	180	30	75	75
T5	240	30	105	105

2.1.2. Acquisition of Hyperspectral Data of the Plant and Analyses of the N Content

Spectral data were measured at 25, 35, 50, and 65 days after emergence (DAE). In each campaign, 10 leaves were acquired from each experimental unit, generating 250 readings per campaign. For standardization purposes in spectral acquisition, fully developed leaves were collected from the upper part of the plant, with the complete detachment of the sheath from the membranous structure. After removal, the middle third of each leaf was cut. In order to maintain turgor for a longer period of time [31], the leaves were placed in plastic bags labeled with their respective identifications and transported in thermal boxes with ice, without direct contact between the leaves and the ice. The entire process, from collection to the readings, was carried out in a maximum of 30 min.

In the laboratory, the spectra were acquired using the spectroradiometer ASD FieldSpec FR Spectroradiometer® (ASD–Analytical Spectral Devices Inc., Boulder, CO, USA) by employing a LeafClip (ASD Inc., Boulder, CO, USA), a device that facilitates spectral readings on the adaxial surface of leaves and reduces the influence of external factors. The spectroradiometer collects data for wavelengths from 350 to 2500 nm, covering the visible (Vis), near-infrared (NIR), and shortwave infrared (SWIR) regions. Once the readings were obtained, the data were exported to the software ViewSpec Pro (ASD—Analytical Spectral Devices Inc., Boulder, CO, USA), where they were converted to reflectance. A data pre-treatment was performed by eliminating the noise from the spectra (350–449 nm), resulting in curves from 450 to 2500 nm.

Subsequently, a composite sample was taken from each plot. The composite samples were sent to the Plant Tissue Laboratory, a sector of the Soil Science Department at University of Sao Paulo (ESALQ/USP), to determine the nitrogen contents for each collection (25, 35, 50, and 65 DAE). The results were obtained in grams of nitrogen per kilogram (g kg^{-1}). The average of the reflectance values corresponding to the same LNC value in each collection (25, 35, 50, and 65 DAE) was calculated. The LNC values were organized in ascending order according to the spectral response.

2.1.3. Spectral Vegetation Indices

Vegetation indices were selected that are sensitive to nitrogen variations, according to the literature. The indices were calculated using the hyperspectral data collected, following the definitions of their authors (Table 2).

Table 2. Vegetation indices tested for their ability to predict leaf nitrogen content in corn.

Index	Name	Formula	Author
Bni	Buschman and Nagel index	$(R_{750} - R_{500})/(R_{750} + R_{500})$	[32]
DCNI	Double-peak canopy nitrogen index	$\left(\frac{R_{720}-R_{700}}{R_{700}-R_{670}}\right)/(R_{670} + 0.03)$	[33]
Gmi_1	Gitelson and Merzlyak index 1	R_{750}/R_{550}	[34]
Gmi_2	Gitelson and Merzlyak index 2	R_{750}/R_{700}	[34]
GNDVI	Green normalized difference vegetation index	$(R_{801} - R_{550})/(R_{801} + R_{550})$	[35]
MCARI	Modified chlorophyll absorption reflectance index	$[(R_{700} - R_{670}) - 0.2 \times (R_{700} - R_{550})] \times \left(\frac{R_{700}}{R_{670}}\right)$	[35]

Table 2. *Cont.*

Index	Name	Formula	Author
MCARI/OSAVI	Modified chlorophyll absorption reflectance index/optimized soil-adjusted vegetation index	$\frac{(3\times[(R_{700}-R_{670})-0.2\times(R_{700}-R_{550})\times(R_{700}-R_{670})])}{((R_{800}-R_{670})\times(1+0.16)/(R_{800}+R_{670}+0.16))}$	[36]
mND_{705}	Modified normal difference index	$(R_{750}-R_{705})/(R_{750}+R_{705}-2\times R_{500})$	[37]
MTCI	MERIS terrestrial chlorophyll index	$(R_{750}-R_{705})/(R_{710}+R_{480})$	[38]
NDCI	Normalized difference chlorophyll index	$(R_{762}-R_{527})/(R_{762}+R_{527})$	[39]
NDDA	Double-peak areas based on REP division	$(R_{755}+R_{680}-2\times R_{705})/(R_{755}-R_{680})$	[40]
NDRE	Normalized difference red-edge index	$(R_{790}-R_{720})/(R_{790}+R_{720})$	[41]
NDVI	Normalized difference vegetation index	$(R_{800}-R_{670})/(R_{800}+R_{670})$	[42]
PSNDa	Pigment-specific normalized difference A	$(R_{800}-R_{680})/(R_{800}+R_{680})$	[43]
PSNDb	Pigment-specific normalized difference B	$(R_{800}-R_{635})/(R_{800}+R_{635})$	[43]
PSNDc	Pigment-specific normalized difference C	$(R_{800}-R_{470})/(R_{800}+R_{470})$	[43]
RI-half	Ratio index—half	R_{744}/R_{708}	[44]
RI-1dB	Ratio index—1 dB	R_{735}/R_{720}	[44]
RI-2dB	Ratio index—2 dB	R_{738}/R_{720}	[44]
RI-3dB	Ratio index—3 dB	R_{741}/R_{717}	[44]

2.1.4. Statistical Analysis of the Data

Partial Least Squares Regression (PLSR)

LNC prediction models were calibrated using the nonlinear interactive PLS algorithm (NIPALS). This technique has the ability to treat correlated independent variables (spectrum wavelengths), reducing them to a set of components while avoiding multicollinearity to estimate a set of dependent variables (LNC) [45]. The LNC prediction models were calibrated individually for each collection date. In parallel, a general prediction was tested, considering the data from the four dates (25, 35, 50, and 65 DAE).

In this study, the data for generating the prediction models were divided into three subsets: (i) from the spectra of all wavelengths (450–2500 nm); (ii) only with the response of the spectral indices; and (iii) through the combination of the bands and vegetative indices. Finally, the bands and spectral indices that were, in fact, relevant in the prediction were defined. Therefore, the variable importance in projection (VIP) was calculated. The VIP values were calculated for each band and spectral index, with only values above 0.8 being considered relevant.

Data Validation

The models were validated using the *k-fold cross-validation* method. This technique first randomly divides the dataset into k subgroups that have approximately the same number of instances. Then, each subgroup, in turn, plays the role of testing the model induced from the other k subgroups [46]. During model calibration, both the model with the optimal number of factors and its respective performance were defined. The best model presented the highest coefficient of determination (R^2), the lowest root mean square error (*RMSE*), and normalized root mean square error (*NRMSE*) which are both described in Equations (1)–(3), respectively.

$$R^2 = \frac{\left[\sum\left(\gamma_p - \overline{\gamma}_p\right)\cdot(\gamma_o - \overline{\gamma}_o)\right]^2}{\sum\left(\gamma_p - \overline{\gamma}_p\right)^2 \cdot \sum(\gamma_o - \overline{\gamma}_o)^2} \quad (1)$$

$$RMSE = \sqrt{\frac{\sum_{i=1}^{n}(\hat{y}_i - y_i)^2}{n}} \quad (2)$$

$$NRMSE = \frac{RMSE}{\overline{y}} \quad (3)$$

In this study, the results were interpreted according to Saeys et al. [47], considering that R^2 values lower than 0.50 were poor; those between 0.50 and 0.65 indicated a reasonable

model, with the possibility of discrimination between high and low concentrations of the modeled attribute; and R^2 values between 0.66 and 0.86 and above 0.86 indicated good and excellent quantitative prediction models, respectively.

3. Results

3.1. Descriptive Analysis of LNCs

Figure 2 represents the mean N levels in each collection (25, 35, 50, and 65 DAE). The nitrogen levels ranged from 42 to 24 g kg^{-1} throughout the collections, in which the highest concentration corresponded to the first collection (25 DAE), with a reduction in the levels as the crop age increased.

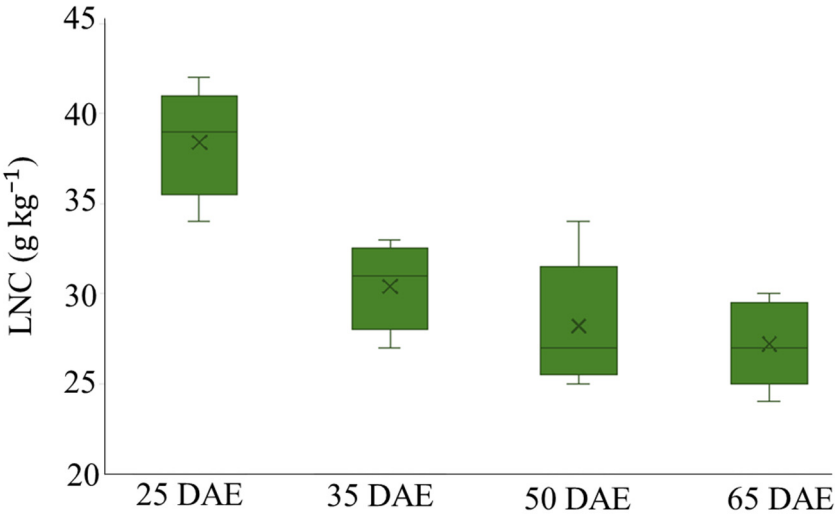

Figure 2. Boxplot graph of the LNC values at 25, 35, 50, and 65 DAE.

3.2. Descriptive Analysis of the Leaf Spectrum

The complete spectrum at 25, 35, 50, and 65 DAE followed a general pattern, with a low reflectance in the Vis region (450–700 nm), a high reflectance in the NIR region (700–1300 nm), and two water absorption peaks (1450 and 1950 nm) in the SWIR region (1300–2500 nm) (Figure 3A–D).

The leaf signatures exhibited a similar behavior throughout the collections, in which the leaves with lower N concentrations exhibited a higher reflectance factor in the visible range, while those with higher N levels showed a lower reflectance, which was more pronounced in the green band (550 nm). This characteristic was observed in all collections in the Vis region (450–700 nm), mainly in the green wavelength (550 nm) (Figure 3(A1–D1)). In the red-edge region, it was possible to visualize the same particularity between the bands corresponding to the highest and lowest content only in the first, third, and last collections (Figure 3(A2,C2,D2)), since, in the second collection (35 DAE), the spectral curves did not distinguish the LNCs (Figure 3(B2)). In contrast, the wavelengths related to NIR (750–1300 nm) followed the LNC pattern only in the first and second collections (Figure 3(A3,B3)), since they were proportional in the last two (50 and 65 DAE), considering the LNC (Figure 3(C3,D3)). The SWIR region, in relation to the initial spectrum (Vis, red-edge, and NIR), was the one that expressed the lowest sensitivity to N, despite presenting a molded behavior in the contents at 35 DAE (Figure 3(B4)).

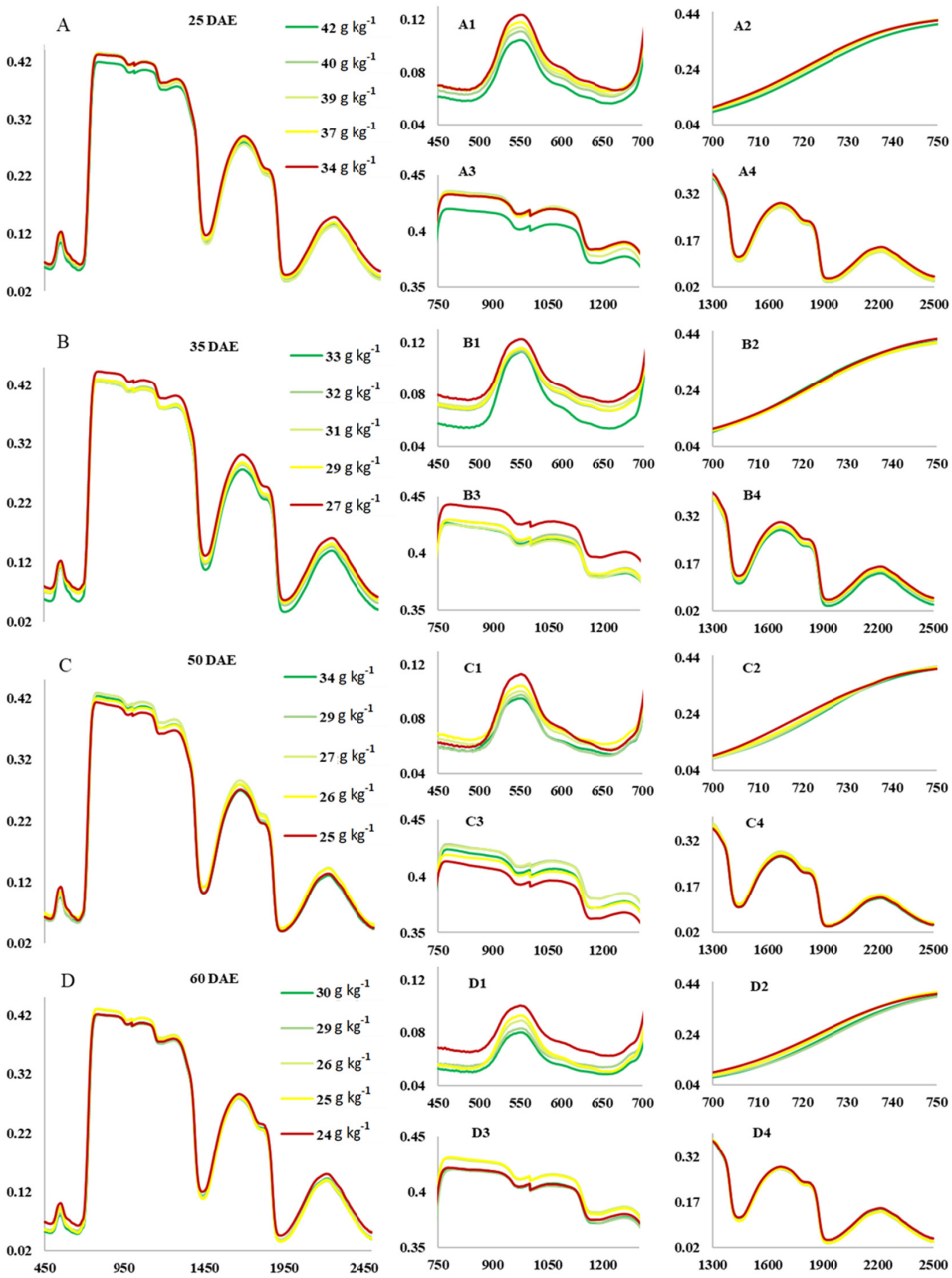

Figure 3. LNC values according to the spectral response of the leaves from the highest to the lowest mean leaf N content at 25, 35, 50, and 65 DAE: complete spectrum (450 to 2500 nm) (**A**–**D**), visible region (450–700 nm) (**A1**–**D1**), red-edge region (700–750 nm) (**A2**–**D2**), and infrared regions: near (750–1300 nm) (**A3**–**D3**) and shortwave (1300–2500 nm) (**A4**–**D4**).

3.3. Performance of Models Using Only Spectra, Vegetation Indices, and General Prediction (Bands + Indices)

Compared with the prediction per band ($0.67 < R^2 < 0.85$ and $1.00 < \text{RMSE} < 1.77$ g kg^{-1}), the VI prediction showed a lower performance, with a reduced R^2 (between 0.55 and 0.68) and an increased RMSE (1.13 and 1.78 g kg^{-1}). In this study, the combination of vegetative indices with spectral bands (450–2500 nm) (general prediction) was also tested as an approach for constructing predictive models. The combination varied between excellent for the first (25 DAE), with an R^2 of 0.87 and an RMSE of 1.50 g kg^{-1}, and good for the other collections (35, 50, and 65 DAE), with an R^2 of 0.74, 0.86, and 0.74 and an RMSE of 1.32, 1.00, and 1.01 g kg^{-1}, respectively (Figure 4).

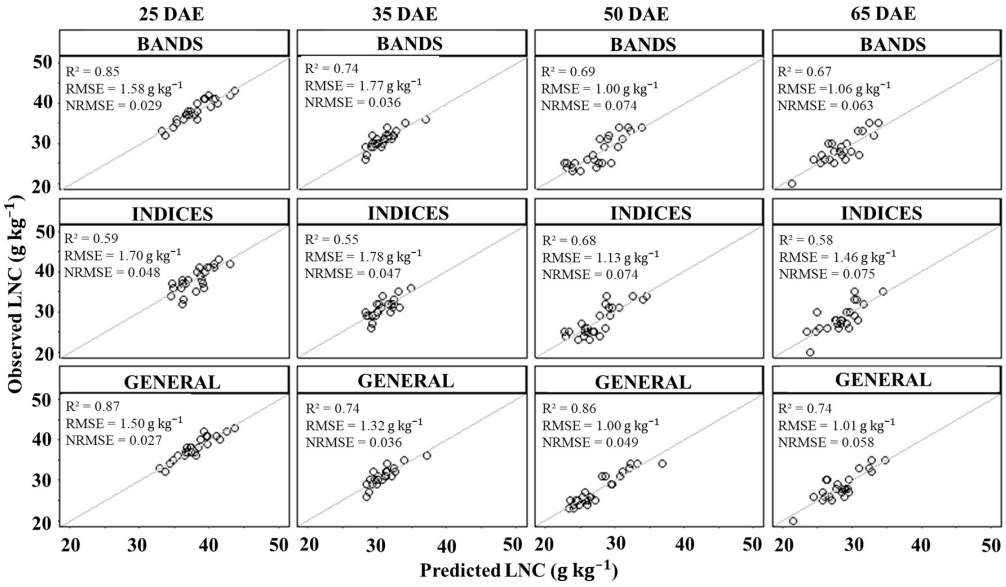

Figure 4. Relationship between observed and predicted LNC: spectral signatures, indices, and overall prediction (bands + indices) using partial least squares regression (PLSR) at 25, 35, 50, and 65 DAE.

The models were developed using all the collected data, resulting in inferior adjustments (Figure 5) compared to the individual models according to the vegetative stages (Figure 4). However, the combination of the spectral bands with the VIs once again generated the best results, with values of R^2 = 0.62 and RMSE = 2.51.

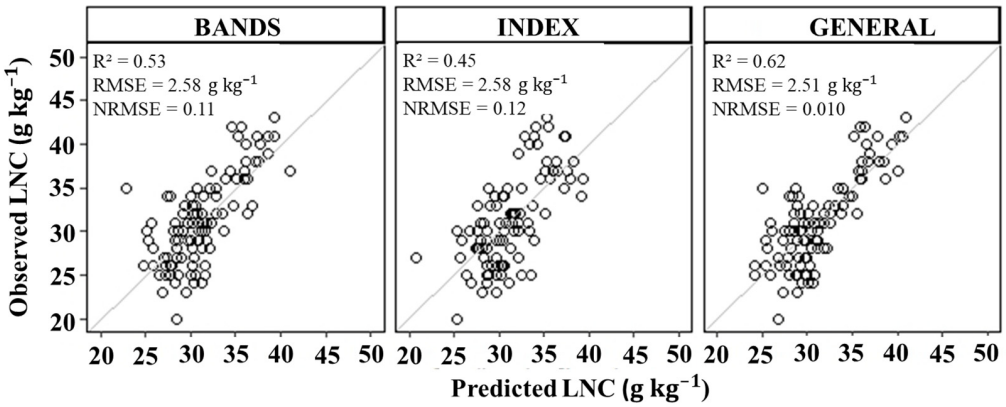

Figure 5. Relationship between observed and predicted LNC, including all collections: spectral signatures, indices, and general prediction (bands + indices), using partial least squares regression (PLSR).

3.4. Variable Importance in Prediction (VIP) of N

3.4.1. Spectral Curves in N Prediction

Using the VIP values, it was possible to identify the most relevant bands and spectral regions in the prediction of N. Based on the VIP threshold score, the most influential regions of the first collection (25 DAE) included the entire Vis region (450–680 nm), with peaks from 450 to 500 nm and at 550 nm; the red-edge region, with the highest-value peak around 700 nm (Figure 6); the NIR region, with a peak close to 1300 nm; and some SWIR bands (1400, 1900, and 2400 nm). In the second (35 DAE) and third (50 DAE) collections, the bands followed the same pattern of importance as the first (25 DAE) in the Vis and red-edge regions. Nonetheless, the wavelengths corresponding to the NIR region (700–1300 nm) did not register relevance in these collections. The importance of the SWIR bands also decreased, with only one peak near 1550 nm at 35 DAE and two peaks (1350 nm and 1500 to 1700 nm) at 50 DAE. The VIP from the fourth collection (65 DAE) presented two peaks in

the Vis region (450 and 550 nm), one peak in the red-edge region (700 nm), one peak in the NIR region (1300 nm), and one peak in the shortwave infrared region at 1600 nm (Figure 6).

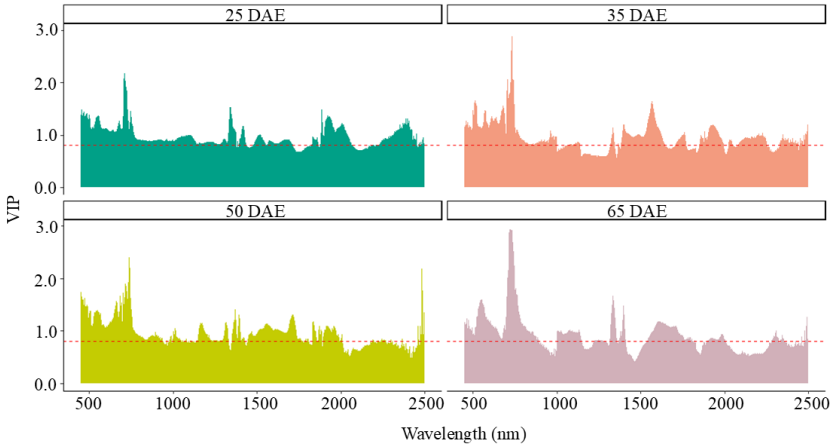

Figure 6. Wavelength variable importance in projection (VIP) scores (dashed red line) at 25, 35, 50, and 65 DAE. Variable relevance > 0.8.

3.4.2. VIs in the Prediction of N

In addition to indicating the most important bands and spectral regions for N predictions, it was also possible to detect the VIs that best contributed to the prediction using the VIP values. There were alternations in the VIP score of each VI throughout the collections. In the first collection (25 DAE), for example, the most relevant indices were Bni, mND_{705}, DCNI, NDRE, Gmi_1, RI-1dB, MTCI, NDDA, MCARI/OSAVI, RI-2dB, MCARI, Gmi_2, PSNDa, PSNDc, NDVI, RI-3dB, and RI-half; in the second (35 DAE), they were Bni, mND_{705}, DCNI, NDRE, Gmi_1, RI-1dB, MTCI, NDDA, MCARI/OSAVI, RI-2dB, MCARI, Gmi_2, PSNDa, NDVI, and PSNDb; in the third (50 DAE), they were Bni, mND_{705}, DCNI, NDRE, Gmi_1, RI-1dB, Gmi_2, PSNDa, PSNDc, NDVI, NDCI, PSNDb, RI-3dB, and GNDVI; and, in the fourth collection (65 DAE), they were Bni, mND_{705}, DCNI, NDRE, Gmi_1, RI-1dB, MTCI, NDDA, MCARI/OSAVI, RI-2dB, MCARI, Gmi_2, and RI-half. Overall, in each specific collection, the VIs demonstrated a moderate divergence in their contribution, except in the third (PSNDa) and fourth (Bni and nDR_{705}) collections, which represented VIs with a greater discrepant importance for the prediction in relation to the others (Figure 7).

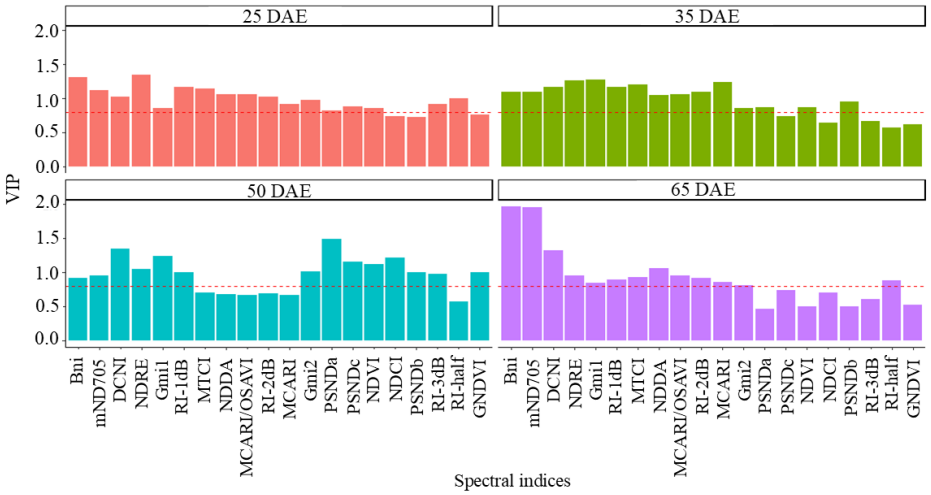

Figure 7. VI variable importance in projection (VIP) scores (dashed red line) at 25, 35, 50, and 65 DAE. Variable relevance > 0.8.

3.4.3. Validation of Band and VI Prediction by Collection

The validation process was performed on the datasets used in the prediction by band and by VI (Figure 8). The model validation generated results similar to the prediction by band, with the peaks and valleys basically in the same regions at 25, 35, 50, and 65 DAE (Figure 8A). On the other hand, for the validation of the VIs, all the indices presented relevance (>0.8) in all collections; nevertheless, the divergence in the magnitude of importance in validation was greater in relation to the VIP score, especially for the first seven indices in the first collection (mND_{705}, DCNI, MCARI, MCARI/OSAVI, Bni, MTCI, and NDDA) and the first five in the second (mND_{705}, DCNI, MCARI, MCARI/OSAVI, and Bni). In the third collection (50 DAE), there was less variation among the VIs, and, in the fourth collection (65 DAE), the first 10 VIs (mND_{705}, DCNI, MCARI, MCARI/OSAVI, Bni, MTCI, NDDA, NDRE, RI-2dB, and RI-1dB) showed prominence compared to the others (Figure 8B).

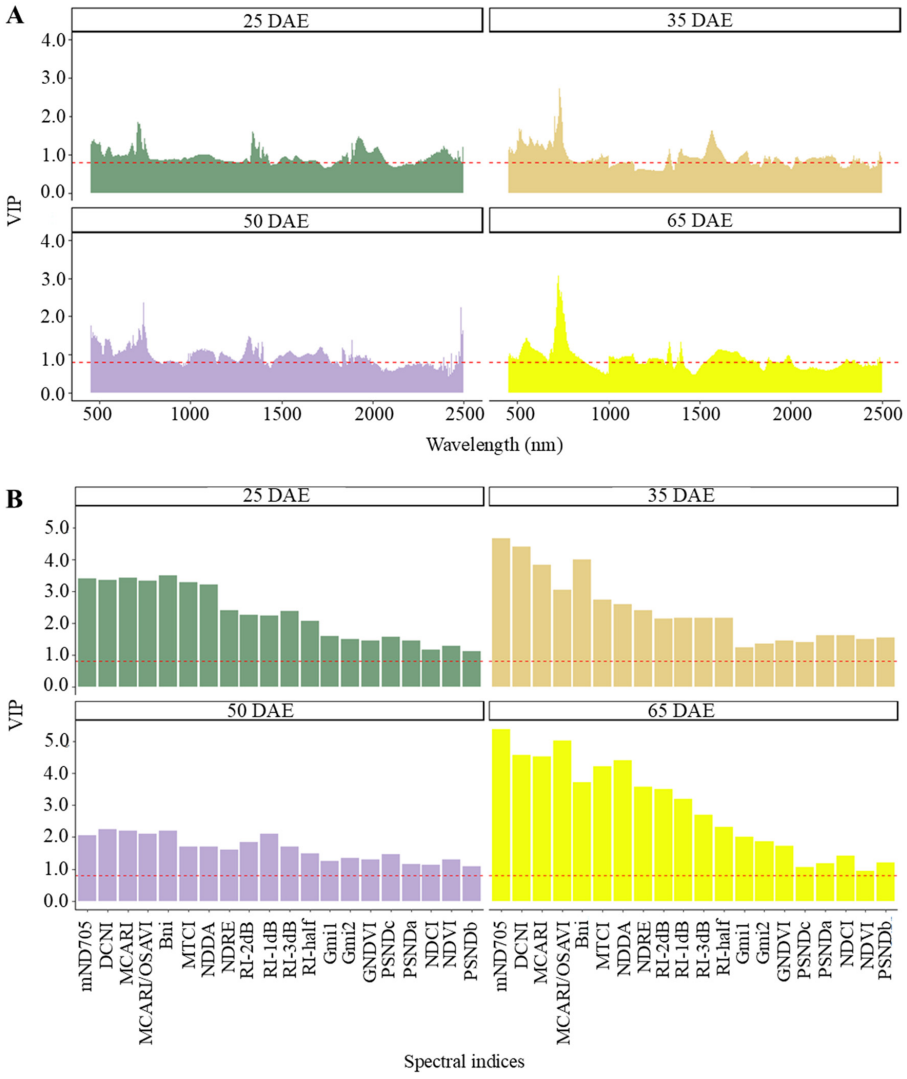

Figure 8. Validation of the dataset used in the predictions by band (**A**) and by index (**B**) at 25, 35, 50, and 65 DAE. Variable relevance > 0.8 (dashed red line).

4. Discussion

4.1. N Content in Corn Plants

Most LNC values fell within the adequate range for corn, remaining at between 35 and 27 g kg^{-1} [48,49] throughout the collections. The reduction in the LNC from the first (42 g kg^{-1}) to the last (24 g kg^{-1}) collection may be related to the vegetative stage of the

plant, due to the contribution of nitrogen in the functions of the different crop stages, such as vegetative growth, biomass production, and the transformation of solar energy [50,51]. From this same perspective, Lee et al. [52] evaluated the LNC in corn and observed a decreasing trend in the levels throughout the cultivation period. Authors such as Davies et al. [53] and Cummings et al. [54] have reported that, physiologically, the N concentration in corn plants is higher at the beginning of their vegetative growth, decreasing until senescence. Chen et al. [55] found similar results; as the corn crop grew, the value of N in the leaves decreased. Similar downward trends have been previously published for the leaf nitrogen curves of crops such as rice [56], winter wheat [57], and corn [58].

4.2. Dynamic Changes in the Leaf Spectrum of Corn Under Different N Levels and at Different Stages

The variability among the curves, especially at 550 nm (green), found in the Vis region (450–700 nm) is strongly linked to leaf pigments and biochemical characteristics [59], while the rest of the spectrum (near-infrared—700 to 1300 nm—and mid-infrared—1300 to 2400 nm) reflects the leaf structural parameters (for instance, dry matter content and leaf thickness) and the water content, respectively [11,60]. This explains the little variation in these bands in response to N. Vis wavelengths are known for their sensitivity to variations in leaf N, indicating that the corn LNC can be observed using reflectance spectroscopy and corroborating previous works in sugarcane [7,16,61,62] and corn [63].

In this study, the red-edge was considered to be between 700 and 750 nm. The domain between the specific bands of the beginning and end of the red-edge may vary depending on the purpose of the analysis, because this band of the spectrum, known in the literature as the inflection point in vegetation reflectance, is the ramp that leads to the rapid increase in reflectance at the final red-edge and initial near-infrared edge [64,65]. For example, Ferwerda, Skidmore [66] observed a change in the position of the red-edge in the deficiency of different nutritional elements (N, P, Ca, K, Na, and Ma). For Barros et al. [61], who evaluated N in sugarcane leaves, the inflection point was determined to be between 710 and 720 nm. Sun et al. [67] reported that the red band is the spectrum most affected by chlorophyll (Chl), which, in turn, undergoes changes according to the supply of N [68], since this is where the maximum Chl absorption occurs; however, this band becomes saturated at high Chl values, which results in a shift in the red-edge domain.

Although the red-edge demonstrated a visibly lower sensitivity compared to the Vis region in response to N in this study, the recognition of this spectral band is noticeable, mainly regarding the highest and lowest LNC (Figure 3(A2–D2)). According to Liang et al. [69] and Peng et al. [70], as with the Vis region, the red-edge characteristics of the vegetation are closely related to the physical and chemical properties, and they contain important information about the vegetation. Authors such as Zhao et al. [71] found bands sensitive to nitrogen in the range between 500 and 710 nm. In the same perspective, Gitelson et al. [72] found that the region with a strong relationship with the chlorophyll and nitrogen levels was 550 nm (green), and this spectral band showed increasing differences throughout their collections, as also observed by Fiorio et al. [7]. Liu et al. [73] evaluated nitrogen in corn using spectral reflectance, but at the canopy level; they reported that the most sensitive bands for monitoring the N concentration were 762 and 726 nm.

In the NIR region (750–1300 nm), which is a spectral range that is related to leaf structure and that indicates whether the plant is gaining biomass in response to nitrogen fertilization [60], both contents reflected values of 35 to 45% in all collections (Figure 3(A3–D3). According to Li et al. [74], the plant's behavior of generating a large difference in absorption and reflectance occurs as protection mechanisms, so that the leaf maintains its energy balance, does not overheat, and avoids chlorophyll malnutrition. Gates et al. [75] reported that the leaf reflectance in this region is the result of the interaction of incident energy with the mesophyll structure. The authors explain that this structure can be modified according to changes in the water–air relationship in the mesophyll due to water availability, thus

altering leaf reflectance, and the lacunosity of the internal leaf structure influences the internal scattering of incident radiation, generating a greater reflectance.

Some studies have reported that internal scattering is influenced by N availability, indicating that higher amounts of N result in a higher reflectance in the NIR region [55,76,77]. Nonetheless, although obvious differences have been observed between the average reflectance levels of a higher and lower content throughout the collections (Figure 3(A3–D3)), in this study, the increase in the average hyperspectral reflectance of corn leaves in the NIR region (750–1300 nm) was lower under low N rates only in the last two collections (50 and 65 DAE). The opposite occurred at the beginning of crop development (25 and 35 DAE). The divergence in the absorption of the mean curves between the first two and the last two collections may be related to the LNC values in the crop at the beginning of development, which were considered to be above the recommended level and which may have caused stress due to the excess of N in the plant. These results provide a theoretical basis that paves the way for further investigation regarding the quantitative relationship between the LNC and the reflectance spectra in the NIR region at different growth stages.

In the SWIR (1300–2500 nm), there were absorption peaks near 1450, 1950, and 2500 nm (Figure 3(A4–D4)), attributes that are related to the presence of water in the leaf [78,79]. According to Rodriguez-Perez et al. [80], the water content in the plant generates absorption in all bands of the spectrum; however, in the shortwave infrared spectrum, these characteristics are more pronounced, mainly around 1450 and 1950 nm. According to Berger et al. [60], the use of spectral data to estimate the N in crops focuses on the Vis and NIR spectral domains, thus neglecting the N related to proteins and nitrogen reallocation for non-photosynthetic behaviors. Nevertheless, in this study, the SWIR region in relation to the initial spectrum (Vis, red-edge, and NIR) was the one that expressed the lowest sensitivity to N, in which the mean signatures overlapped without dissonance between the contents. However, at 35 DAE (Figure 3(B4)), the behavior of the curves was shaped (Figure 3(B4)), with a tendency to increase the reflectance of the lowest content in the other collections.

4.3. Prediction of N by Spectral Band and by VI

The R^2 values were interpreted according to Saeys et al. [47]. The prediction by band generated results that were considered good in all the collections (25, 35, 50, and 65 DAE), with R^2 values ranging from 0.67 to 0.85 and an RMSE between 1.00 and 1.77 g kg^{-1}. However, the prediction by VI was considered reasonable, since the R^2 decreased to 0.59, 0.55, 0.68, and 0.58 and the RMSE increased to 1.70, 1.78, 1.13, and 1.46 g kg^{-1} at 25, 35, 50, and 65 DAE, respectively. An exception was the third collection (50 DAE), which presented the highest R^2 (0.68) and the lowest RMSE (1.13 g kg^{-1}); these values were considered good (Figure 4).

The PLSR proved to be favorable in the prediction using hyperspectral data and vegetation indices, since it resulted in an $R^2 > 0.54$ and an RMSE < 1.79 g kg^{-1} (Figure 4). Nevertheless, the performance patterns of the predictive models revealed variations, which were intrinsically associated with the specific vegetative stage of the crop and the datasets used in the modeling. For example, at the stage of 25 DAE (V4), the models (R^2 = 0.85) exhibited a better adaptability when built only with the spectral bands (450 to 2500 nm). On the other hand, for the other collection dates (35, 50, and 65 DAE), the models exhibited similar R^2 values (0.74, 0.69, and 0.67, respectively). This fact may be correlated with the LNC of the crop, since the highest levels (Figures 2 and 3A) were found in the first collection (25 DAE), while the rates at 35, 50, and 65 DAE were similar. According to Davies et al. [53], the N consumption by corn plants during the initial vegetative stages was low, increasing rapidly as the plant developed, which explains the variation in the LNC.

Fan et al. [81] succeeded (R^2 = 0.77) in applying the same method (PLSR) for predicting the N concentration using spectral curves acquired from corn plants. Other researchers have also evaluated the prediction of leaf characteristics, including the N concentration in corn, and achieved an R^2 of 0.96 [17]. However, in this study, different periods of corn

development were evaluated (25, 35, 50, and 65 DAE), of which the collection performed at 65 DAE (V10) resulted in the lowest R^2 (0.67) in the prediction by band (Figure 4). This is an event that may be linked to the crop phase in this collection (beginning of flowering) when the tassel appears, indicating that the plant has reached its maximum height, with nutrients being reallocated for grain production [82]. In this phase, the remobilization of the reserves present in the stem and leaves occurs to adequately and successively support the next cycles (flowering and grain filling) [83], which explains the reduction in the LNC at the end of the cycle.

In the models based on the VI responses, the development stage V10 (50 DAE) presented the best adaptation (R^2 = 0.68), which was characterized by the accumulation of as much N as possible for later reallocation according to the subsequent phenological stages (between V10 and V14) [84]. This explains the highest R^2 at this stage. In addition, the index prediction generated the lowest R^2 values (0.59, 0.55, 0.68, and 0.58, respectively) and the highest RMSE values (1.70, 1.78, 1.13, and 1.46, respectively) for the collections (25, 35, 50, and 65 DAE) when compared to the band prediction (Figure 4). Overall, the performance of the VI may be related to the fact that the VI calculation considers only a few spectral bands, and ends up losing information hidden in other wavelengths. Mahajan et al. [85] reported that the use of a few wavelengths in vegetation spectral indices for nutrient predictions offers a simple way to model any parameter, but, at the same time, it does not give attention to information that may be present in other bands of the spectrum. Yang et al. [86] used PLSR to predict the canopy nitrogen in several crops and found an R^2 = 0.97 for the bands and an R^2 = 0.96 for VIs in corn plants. This corroborates the results demonstrated here, in which the prediction by VI was lower. Peng et al. [87] evaluated several VIs and found an $R^2 > 0.50$ when studying N in shrubs and grasses. Xia et al. [88] estimated the N status by VI and found an R^2 between 0.56 and 0.65 at the growth stages V7 and V10; their results are similar to those of this research.

The synergy between the spectral bands and the VIs (general prediction) acted as a complement, resulting in significant improvements in the values of $R^2 > 0.73$ and in the reduction in the RMSE < 1.51 g kg^{-1}. This indicates that the model (PLSR) responded better when combining the variables, which is in agreement with the results of Chemura et al. [89], who found results of R^2 = 0.78 and RMSE = 0.23 in the same combination when evaluating the N in coffee. Finally, models were developed using all the data collected, resulting in inferior fits (Figure 4) compared to the individual models by vegetative stages (Figure 3). However, the combination of the spectral bands with the vegetative indices demonstrated the best results once again, with values of R^2 = 0.62 and RMSE = 2.51, highlighting the effectiveness of the combination of spectral bands with additional variables.

4.4. Potential of the Evaluated Models

The most important spectral zones (Vis, red-edge, NIR, and SWIR) according to the VIP variable in the first collection (25 DAE) were observed from 450 to 500 nm and at 550, 700, 1300, 1400, 1900, and 2400 nm. At 35 and 50 DAE, the signatures followed a pattern of importance similar to the first collection; however, the wavelengths corresponding to the NIR region (700–1300 nm) did not register relevance in these collections. The importance of the SWIR bands also decreased, with only one peak close to 1550 nm at 35 DAE and two peaks (1350 nm and 1500 to 1700 nm) at 50 DAE. In the fourth collection (65 DAE), the VIP presented two peaks in the Vis region (450 and 550 nm), one peak in the red-edge region (700 nm), one peak in the NIR region (1300 nm), and two peaks in the shortwave infrared region at 1600 nm (Figure 6). This panorama highlights the importance of the Vis (450–700 nm) and red-edge (700–750 nm) bands in the prediction by band, since they represent the amplitude of importance in all collections. These results corroborate those found by Fiorio et al. [7], who evaluated the leaf nitrogen in sugarcane; in their study, the authors reported that the most important spectral bands were in the visible and red-edge regions. Authors such as Shiratsuchi et al. [90] emphasize that red-edge is a powerful and temporally stable region that directly contributes to the estimation of the N status of a crop.

Azadnia et al. [91] found bands of greater importance in estimating the leaf N content in the visible region (510–540 nm and 670–690 nm).

The importance of different VIs varied according to the growth stages and N status indicators. The magnitude of the indices in the VIP score throughout the collections can be influenced by many factors, including crop growth stages [13]. According to Hatfield, Hatfield and Prueger [92], and Gnyp et al. [93], the growth stage can strongly interfere with the sensitivity and performance of different VIs to estimate crop parameters. The reduction in or appearance of particles on the leaf throughout the life of the crop alters the reflectance [94]. For example, in the first two collections (25 and 35 DAE) of the 20 VIs tested in this study, none highlighted a discrepancy in the predictions. Even when presenting a relevance above 0.8, both generated similar performances (between 1.0 and 1.4), except for those that did not contribute in the first (NDCI, PSNDb, and GNDVI) or second (PSNDc, NDCI, and RI-3db) collection (Figure 7). This indicates difficulty in choosing a VI to estimate N in the initial growth stages.

Nevertheless, from the third collection onwards, the VIs showed a greater divergence in their contribution, with an emphasis on PSNDa in the third and Bni and nDR_{705} in the fourth collection. Li et al. [77] obtained similar results when evaluating the use of hyperspectral vegetation indices to estimate the nitrogen content in wheat at different growth stages. The authors emphasized that, in the initial growth stages of the plant (between V4 and V7), the VIs generated a lower efficiency. According to Haboudane et al. [36], in the initial stages, leaf development is greater and can mask the effects of chlorophyll and N, since the aim in these periods is plant development. In the later stages, these effects may decrease, since the aim is grain development.

A very interesting phenomenon found in this study is that the wavelengths that composed the most effective VIs in the first (Bni, mND_{705}, DCNI, NDRE, Gmi_1, RI-1dB, MTCI, NDDA, MCARI/OSAVI, RI-2dB, MCARI, Gmi_2, PSNDa, PSNDc, NDVI, RI-3dB, and RI-half), second (Bni, mND_{705}, DCNI, NDRE, Gmi_1, RI-1dB, MTCI, NDDA, MCARI/OSAVI, RI-2dB, MCARI, Gmi_2, PSNDa, NDVI, and PSNDb), third (Bni, mND_{705}, DCNI, NDRE, Gmi_1, RI-1dB, Gmi_2, PSNDa, PSNDc, NDVI, NDCI, PSNDb, RI-3dB, and GNDVI), and fourth (Bni, mND_{705}, DCNI, NDRE, Gmi_1, RI-1dB, MTCI, NDDA, MCARI/OSAVI, RI-2dB, MCARI, Gmi_2, and RI-half) collections, selected using the VIP variable, were basically consistent with the most important spectral bands in the per-band prediction, indicating that these wavelengths are the most important for both predictions.

4.5. Prediction Quality

The adopted validation method returned similar predictions according to the configuration defined by the model (PLSR) when predicting the LNC in corn. The configurations are indicative of the importance of spectral bands and VIs in predicting this agronomic variable. Nonetheless, the performance of the data was better evaluated in the synergy of the attributes (general prediction) when considering different stages (25, 35, 50, and 65 DAE), as discussed. This characteristic occurs mainly because, when combining spectral bands and VIs, a prominence is verified in some characteristics related to biological variables, such as the chlorophyll content and biomass, demonstrating a lesser degree of performance when modeled individually [95]. This type of evaluation is important because it allows the input variables that are most suitable for modeling the problem to be indicated, resulting in a more accurate estimate [95]. The accuracy of PLSR models in estimating N is extremely powerful, since this method explores and evaluates the relationship between scales of nutrient characteristics, resolves multicollinearity problems between variables, and performs a principal component analysis on the matrices of independent and dependent variables [96]. Some studies have reported that the predictive power of PLSR is strong and robust, shedding light on approaches related to N predictions [81,96,97].

4.6. Limitations and Future Work

This study showed promising results for CLN prediction using spectroscopy, but some issues still need to be addressed. Inferring plant N status from leaf or canopy data alone can be problematic. N interactions in soil-plant systems are complex and directly related to many physiological processes, including respiration, structural growth, and storage capacity building [98]. In corn, N is stored in vegetative tissues (leaves and stalks) during the growth phase but is partially translocated to ears and grains during the reproductive phase [99]. Depending on the crop phenological stage in which the leaves/canopy spectra are measured, their relationship with corn N status might not be consistent. Previous studies [11] indicated that even multi-temporal vegetation indices cannot describe relationships between spectral data and N translocation in crops. Once that remotely sensed data cannot detect N translocation into the grain, the grain protein content is also not reliably predicted from canopy spectral measurements. Therefore, the dynamic nature of N in soil-plant systems adds a complexity in accurately assessing the crop N status using canopy remotely sensed data, and, consequently, developing effective N management strategies for in-season correction [98].

Another issue is the validation of our prediction models. In our case, we used 10-fold cross-validation (CV), which is statistically sound and has been extensively described in the statistical and environmental literature [100]. However, some recent studies claim that accuracy indices obtained using CV are biased because calibration points are not statistically independent of validation points [101]. Ideally, these models should be evaluated with an independent dataset and their performance assessed against data from different years, phenological stages, or sites with different environmental conditions. This type of validation simulates conditions that are closer to reality in a crop field, where pre-calibrated models would be used to predict N under unknown conditions [7]. Unfortunately, in our study, we were not able to replicate the field experiments across multiple sites and years. Future work should focus on testing N prediction models under different environmental conditions and in years with different climatic conditions.

5. Conclusions

In this study, the potential of using Vis-NIR-SWIR spectral data as the input variable to predict the LNC in corn plants was investigated. The results showed that the combination of spectral bands and VIs (overall prediction) resulted in an efficient prediction ($R^2 > 0.74$ and reduced RMSE < 1.50 g kg^{-1}) by the specific crop stage, compared to individual predictions (bands or VIs). Additionally, this study demonstrates how hyperspectral data offer a new opportunity to monitor the leaf nitrogen content. This could assist the development of techniques for large-scale nutrient management, mainly in the spectral bands from 450 to 750 nm, since these were the bands that were most sensitive to N.

Author Contributions: Conceptualization, A.K.d.S.O. and P.R.F.; methodology, A.K.d.S.O., R.R., C.A.A.C.S. and N.C.R.; software, A.K.d.S.O., R.R. and C.A.A.C.S.; validation, A.K.d.S.O., C.A.A.C.S. and M.L.C.; formal analysis, A.K.d.S.O., C.A.A.C.S., N.C.R. and P.R.F.; investigation, A.K.d.S.O. and N.C.R.; resources, P.R.F.; data curation, P.R.F.; writing—original draft preparation, A.K.d.S.O., R.R., C.A.A.C.S. and P.R.F.; writing—review and editing, A.K.d.S.O., R.R., C.A.A.C.S., M.L.C. and P.R.F.; visualization, A.K.d.S.O. and P.R.F.; supervision, P.R.F.; project administration, P.R.F.; funding acquisition, P.R.F. All authors have read and agreed to the published version of the manuscript.

Funding: This research was funded by São Paulo Research Foundation (FAPESP) grant number 2013/22435-9. The A.K.d.S.O was funded by Coordination for the Improvement of Higher Education Personnel (Capes).

Data Availability Statement: The data that support the findings of this study are available from the corresponding author upon reasonable request.

Conflicts of Interest: The authors declare no conflicts of interest.

References

1. Deng, H.; Zheng, W.; Shen, Z.; Štreimikienė, D. Does fiscal expenditure promote green agricultural productivity gains: An investigation on corn production. *Appl. Energy* **2023**, *334*, 120666. [CrossRef]
2. Wilhelm, W.W.; Johnson, J.M.F.; Hatfield, J.L.; Voorhees, W.B.; Linden, D.R. Crop and Soil Productivity Response to Corn Residue Removal: A Literature Review. *Agron. J.* **2004**, *96*, 1–17. [CrossRef]
3. Ransom, C.J.; Kitchen, N.R.; Camberato, J.J.; Carter, P.R.; Ferguson, R.B.; Fernández, F.G.; Franzen, D.W.; Laboski, C.A.M.; Nafziger, E.D.; Sawyer, J.E.; et al. Corn nitrogen rate recommendation tools' performance across eight US midwest corn belt states. *Agron. J.* **2020**, *112*, 470–492. [CrossRef]
4. Misbah, K.; Laamrani, A.; Khechba, K.; Dhiba, D.; Chehbouni, A. Multi-sensors remote sensing applications for assessing, monitoring, and mapping NPK content in soil and crops in African agricultural land. *Remote Sens.* **2021**, *14*, 81. [CrossRef]
5. Patel, A.K.; Ghosh, J.K.; Sayyad, S.U. Fractional abundances study of macronutrients in soil using hyperspectral remote sensing. *Geocarto Int.* **2022**, *37*, 474–493. [CrossRef]
6. Sabzi, S.; Pourdarbani, R.; Rohban, M.H.; García-Mateos, G.; Arribas, J.I. Estimation of nitrogen content in cucumber plant (*Cucumis sativus* L.) leaves using hyperspectral imaging data with neural network and partial least squares regressions. *Chemom. Intell. Lab. Syst.* **2021**, *217*, 104404. [CrossRef]
7. Fiorio, P.R.; Silva, C.A.A.C.; Rizzo, R.; Demattê, J.A.M.; Luciano, A.C.d.S.; da Silva, M.A. Prediction of leaf nitrogen in sugarcane (*Saccharum* spp.) by Vis-NIR-SWIR spectroradiometry. *Heliyon* **2024**, *10*, e26819. [CrossRef]
8. Wang, S.; Guan, K.; Wang, Z.; Ainsworth, E.A.; Zheng, T.; A Townsend, P.; Li, K.; Moller, C.; Wu, G.; Jiang, C. Unique contributions of chlorophyll and nitrogen to predict crop photosynthetic capacity from leaf spectroscopy. *J. Exp. Bot.* **2021**, *72*, 341–354. [CrossRef] [PubMed]
9. Martins, J.A.; Fiorio, P.R.; Barros, P.P.d.S.; Demattê, J.A.M.; Molin, J.P.; Cantarella, H.; Neale, C.M.U. Potential use of hyperspectral data to monitor sugarcane nitrogen status. *Acta Sci. Agron.* **2020**, *43*, e47632. [CrossRef]
10. Rambo, L.; Ma, B.; Xiong, Y.; da Silvia, P.R.F. Leaf and Canopy Optical Characteristics as Crop-N-Status Indicators for Field Nitrogen Management in Corn. *J. Plant Nutr. Soil Sci.* **2010**, *173*, 434–443. [CrossRef]
11. Xue, L.-H.; Cao, W.-X.; Yang, L.-Z. Predicting Grain Yield and Protein Content in Winter Wheat at Different N Supply Levels Using Canopy Reflectance Spectra. *Pedosphere* **2007**, *17*, 646–653. [CrossRef]
12. Long, S.P.; Marshall-Colon, A.; Zhu, X.-G. Meeting the global food demand of the future by engineering crop photosynthesis and yield potential. *Cell* **2015**, *161*, 56–66. [CrossRef] [PubMed]
13. Kizilgeci, F.; Yildirim, M.; Islam, M.S.; Ratnasekera, D.; Iqbal, M.A.; EL Sabagh, A. Normalized difference vegetation index and chlorophyll content for precision nitrogen management in durum wheat cultivars under semi-arid conditions. *Sustainability* **2021**, *13*, 3725. [CrossRef]
14. Wang, X.; Miao, Y.; Dong, R.; Zha, H.; Xia, T.; Chen, Z.; Kusnierek, K.; Mi, G.; Sun, H.; Li, M. Machine learning-based in-season nitrogen status diagnosis and side-dress nitrogen recommendation for corn. *Eur. J. Agron.* **2021**, *123*, 126193. [CrossRef]
15. Soltanikazemi, M.; Minaei, S.; Shafizadeh-Moghadam, H.; Mahdavian, A. Field-scale estimation of sugarcane leaf nitrogen content using vegetation indices and spectral bands of Sentinel-2: Application of random forest and support vector regression. *Comput. Electron. Agric.* **2022**, *200*, 107130. [CrossRef]
16. Zha, H.; Miao, Y.; Wang, T.; Li, Y.; Zhang, J.; Sun, W.; Feng, Z.; Kusnierek, K. Improving unmanned aerial vehicle remote sensing-based rice nitrogen nutrition index prediction with machine learning. *Remote Sens.* **2020**, *12*, 215. [CrossRef]
17. Osco, L.P.; Ramos, A.P.M.; Pereira, D.R.; Moriya, A.S.; Imai, N.N.; Matsubara, E.T.; Estrabis, N.; de Souza, M.; Junior, J.M.; Gonçalves, W.N.; et al. Predicting canopy nitrogen content in citrus-trees using random forest algorithm associated to spectral vegetation indices from UAV-imagery. *Remote Sens.* **2019**, *11*, 2925. [CrossRef]
18. Barbedo, J.G.A. Detection of nutrition deficiencies in plants using proximal images and machine learning: A review. *Comput. Electron. Agric.* **2019**, *162*, 482–492. [CrossRef]
19. Silva, C.A.A.C.; Fiorio, P.R.; Rizzo, R.; Rossetto, R.; Vitti, A.C.; Dias, F.L.F.; de Oliveira, K.A.; Neto, M.B. Detection of nutritional stress in sugarcane by VIS-NIR-SWIR reflectance spectroscopy. *Cienc. Rural* **2023**, *53*, e20220543. [CrossRef]
20. Yendrek, C.R.; Tomaz, T.; Montes, C.M.; Cao, Y.; Morse, A.M.; Brown, P.J.; McIntyre, L.M.; Leakey, A.D.B.; Ainsworth, E.A. High-Throughput Phenotyping of Maize Leaf Physiological and Biochemical Traits Using Hyperspectral Reflectance. *Plant Physiol.* **2017**, *173*, 614–626. [CrossRef]
21. Wu, J.; Rogers, A.; Albert, L.P.; Ely, K.; Prohaska, N.; Wolfe, B.T.; Oliveira, R.C.; Saleska, S.R.; Serbin, S.P. Leaf reflectance spectroscopy captures variation in carboxylation capacity across species, canopy environment and leaf age in lowland moist tropical forests. *New Phytol.* **2019**, *224*, 663–674. [CrossRef] [PubMed]
22. Li, X.; Ba, Y.; Zhang, S.; Nong, M.; Zhang, M.; Wang, C. Sugarcane Nitrogen and Irrigation Level Prediction Based on UAV-Captured Multispectral Images at the Elongation Stage. *bioRxiv* **2020**. [CrossRef]
23. Ge, H.; Xiang, H.; Ma, F.; Li, Z.; Qiu, Z.; Tan, Z.; Du, C. Estimating plant nitrogen concentration of rice through fusing vegetation indices and color moments derived from UAV-RGB images. *Remote Sens.* **2021**, *13*, 1620. [CrossRef]
24. Vollmann, J.; Rischbeck, P.; Pachner, M.; Đorđević, V.; Manschadi, A.M. High-throughput screening of soybean di-nitrogen fixation and seed nitrogen content using spectral sensing. *Comput. Electron. Agric.* **2022**, *199*, 107169. [CrossRef]
25. Li, Y.; Sun, H.; Tomasetto, F.; Jiang, J.; Luan, Q. Spectrometric Prediction of Nitrogen Content in Different Tissues of Slash Pine Trees. *Plant Phenomics* **2022**, *2022*, 9892728. [CrossRef]

26. Zhang, Z.; Jin, W.; Dou, R.; Cai, Z.; Wei, H.; Wu, T.; Yang, S.; Tan, M.; Li, Z.; Wang, C.; et al. Improved Estimation of Leaf Area Index by Reducing Leaf Chlorophyll Content and Saturation Effects Based on Red-Edge Bands. *IEEE Trans. Geosci. Remote Sens.* **2023**, *61*, 4403314. [CrossRef]
27. Silva, F.; Wijewardane, N.K.; Bheemanahalli, R.; Reddy, K.R.; Zhang, X.; Vennam, R.R. Comparison of UV, visible and near-infrared, and mid-infrared spectrometers to estimate maize and sorghum leaf nutrients using dry-intact and ground leaves. *Comput. Electron. Agric.* **2023**, *211*, 108001. [CrossRef]
28. Xie, C.Q.; Yang, C.; Hummel, A.; Johnson, G.A.; Izuno, F.T. Spectral reflectance response to nitrogen fertilization in field grown corn. *Int. J. Agric. Biol. Eng.* **2018**, *11*, 118–126. [CrossRef]
29. World Reference Base for Soil Resources. *International Soil Classification System for Naming Soils and Creating Legends for Soil Maps*; LLC MAKS Press: Moscow, Russia, 2024. [CrossRef]
30. Alvares, C.A.; Stape, J.L.; Sentelhas, P.C.; Moraes, G.J.L.; Sparovek, G. Köppen's climate classification map for Brazil. *Meteorol. Z.* **2013**, *22*, 711–728. [CrossRef]
31. Tavares, T.R.; Fiorio, P.R.; Seixas, H.T.; Garcia, A.C.; Barros, P.P.d.S. Effects of storage on vis-NIR-SWIR reflectance spectra of Mombasa grass leaf samples. *Cienc. Rural* **2020**, *50*. [CrossRef]
32. Buschmann, C.; Nagel, E. In vivo spectroscopy and internal optics of leaves as basis for remote sensing of vegetation. *Int. J. Remote Sens.* **1993**, *14*, 711–722. [CrossRef]
33. Chen, P.; Haboudane, D.; Tremblay, N.; Wang, J.; Vigneault, P.; Li, B. New spectral indicator assessing the efficiency of crop nitrogen treatment in corn and wheat. *Remote Sens. Environ.* **2010**, *114*, 1987–1997. [CrossRef]
34. Gitelson, A.A.; Merzlyak, M.N. Quantitative estimation of chlorophyll-a using reflectance spectra: Experiments with autumn chestnut and maple leaves. *J. Photochem. Photobiol. B Biol.* **1994**, *22*, 247–252. [CrossRef]
35. Daughtry, C.S.T.; Walthall, C.L.; Kim, M.S.; De Colstoun, E.B.; McMurtrey, J.E., III. Estimating Corn Leaf Chlorophyll Concentration from Leaf and Canopy Reflectance. *Remote Sens. Environ.* **2000**, *74*, 229–239. [CrossRef]
36. Haboudane, D.; Miller, J.R.; Tremblay, N.; Zarco-Tejada, P.J.; Dextraze, L. Integrated narrow-band vegetation indices for prediction of crop chlorophyll content for application to precision agriculture. *Remote Sens. Environ.* **2002**, *81*, 416–426. [CrossRef]
37. A Sims, D.; A Gamon, J. Relationships between leaf pigment content and spectral reflectance across a wide range of species, leaf structures and developmental stages. *Remote Sens. Environ.* **2002**, *81*, 337–354. [CrossRef]
38. Dash, J.; Curran, P.J. The MERIS terrestrial chlorophyll index. *Int. J. Remote Sens.* **2004**, *25*, 5403–5413. [CrossRef]
39. Marshak, A.; Knyazikhin, Y.; Davis, A.; Wiscombe, W.; Pilewskie, P. Cloud-vegetation interaction: Use of normalized difference cloud index for estimation of cloud optical thickness. *Geophys. Res. Lett.* **2000**, *27*, 1695–1698. [CrossRef]
40. Feng, W.; Guo, B.-B.; Wang, Z.-J.; He, L.; Song, X.; Wang, Y.-H.; Guo, T.-C. Measuring leaf nitrogen concentration in winter wheat using double-peak spectral reflection remote sensing data. *Field Crops Res.* **2014**, *159*, 43–52. [CrossRef]
41. Barnes, E.; Colaizzi, P.; Haberland, J.; Waller, P. Coincident Detection of Crop Water Stress, Nitrogen Status, and Canopy Density Using Ground Based Multispectral Data. 2000. Available online: https://www.researchgate.net/publication/43256762 (accessed on 5 June 2024).
42. Rouse, J.W.; Hass, R.H.; Schell, J.A.; Deering, D.W.; Harlan, J.C. *Monitoring the Vernal Advancement and Retrogradation (Greenwave Effect) of Natural Vegetation*; NASA/GSFC Type III Final Report; NASA/GSFC: Greenbelt, MD, USA, 1974. Available online: https://ntrs.nasa.gov/citations/19750020419 (accessed on 5 June 2024).
43. Blackburn, G.A. Quantifying Chlorophylls and Caroteniods at Leaf and Canopy Scales: An Evaluation of Some Hyperspectral Approaches. *Remote Sens. Environ.* **1998**, *66*, 273–285. [CrossRef]
44. Gupta, R.; Vijayan, D.; Prasad, T. Comparative analysis of red-edge hyperspectral indices. *Adv. Space Res.* **2003**, *32*, 2217–2222. [CrossRef]
45. Reyes-Trujillo, A.; Daza-Torres, M.C.; Galindez-Jamioy, C.A.; Rosero-García, E.E.; Muñoz-Arboleda, F.; Solarte-Rodriguez, E. Estimating canopy nitrogen concentration of sugarcane crop using in situ spectroscopy. *Heliyon* **2021**, *7*, e06566. [CrossRef]
46. Wong, T.-T.; Yeh, P.-Y. Reliable Accuracy Estimates from *k*-Fold Cross Validation. *IEEE Trans. Knowl. Data Eng.* **2020**, *32*, 1586–1594. [CrossRef]
47. Saeys, W.; Mouazen, A.; Ramon, H. Potential for Onsite and Online Analysis of Pig Manure using Visible and Near Infrared Reflectance Spectroscopy. *Biosyst. Eng.* **2005**, *91*, 393–402. [CrossRef]
48. Malavolta, E.; Vitti, G.C.; Oliveira, S.A. *Evaluation of Plant Nutritional Status: Principles and Applications*; POTAFOS: Piracicaba, Brazil, 1997.
49. Van Raij, B.; Cantarella, H.; Quaggio, J.A.; Furlani, A.M.C. *Recomendações de Adubação e Calagem para o Estado de São Paulo*, 1st ed.; Instituto Agronomico de Campinas: Campinas, Brazil, 1997.
50. Campos, I.; González-Gómez, L.; Villodre, J.; González-Piqueras, J.; Suyker, A.E.; Calera, A. Remote sensing-based crop biomass with water or light-driven crop growth models in wheat commercial fields. *Field Crops Res.* **2018**, *216*, 175–188. [CrossRef]
51. Yue, J.; Yang, G.; Li, C.; Li, Z.; Wang, Y.; Feng, H.; Xu, B. Estimation of winter wheat above-ground biomass using unmanned aerial vehicle-based snapshot hyperspectral sensor and crop height improved models. *Remote Sens.* **2017**, *9*, 708. [CrossRef]
52. Lee, H.; Wang, J.; Leblon, B. Using linear regression, random forests, and support vector machine with unmanned aerial vehicle multispectral images to predict canopy nitrogen weight in corn. *Remote Sens.* **2020**, *12*, 2071. [CrossRef]
53. Davies, B.; Coulter, J.A.; Pagliari, P.H. Timing and rate of nitrogen fertilization influence maize yield and nitrogen use efficiency. *PLoS ONE* **2020**, *15*, e0233674. [CrossRef]

54. Cummings, C.; Miao, Y.; Paiao, G.D.; Kang, S.; Fernández, F.G. Corn nitrogen status diagnosis with an innovative multi-parameter crop circle phenom sensing system. *Remote Sens.* **2021**, *13*, 401. [CrossRef]
55. Chen, B.; Lu, X.; Yu, S.; Gu, S.; Huang, G.; Guo, X.; Zhao, C. The Application of Machine Learning Models Based on Leaf Spectral Reflectance for Estimating the Nitrogen Nutrient Index in Maize. *Agriculture* **2022**, *12*, 1839. [CrossRef]
56. Yao, X.; Ata-Ul-Karim, S.T.; Zhu, Y.; Tian, Y.; Liu, X.; Cao, W. Development of critical nitrogen dilution curve in rice based on leaf dry matter. *Eur. J. Agron.* **2014**, *55*, 20–28. [CrossRef]
57. Yao, X.; Zhao, B.; Tian, Y.C.; Liu, X.J.; Ni, J.; Cao, W.X.; Zhu, Y. Using leaf dry matter to quantify the critical nitrogen dilution curve for winter wheat cultivated in eastern China. *Field Crops Res.* **2014**, *159*, 33–42. [CrossRef]
58. Sieling, K.; Kage, H. Organ-specific critical N dilution curves and derived NNI relationships for winter wheat, winter oilseed rape and maize. *Eur. J. Agron.* **2021**, *130*, 126365. [CrossRef]
59. Hank, T.B.; Berger, K.; Bach, H.; Clevers, J.G.; Gitelson, A.; Zarco-Tejada, P.; Mauser, W. Spaceborne Imaging Spectroscopy for Sustainable Agriculture: Contributions and Challenges. *Surv. Geophys.* **2019**, *40*, 515–551. [CrossRef]
60. Berger, K.; Verrelst, J.; Féret, J.-B.; Wang, Z.; Wocher, M.; Strathmann, M.; Danner, M.; Mauser, W.; Hank, T. Crop nitrogen monitoring: Recent progress and principal developments in the context of imaging spectroscopy missions. *Remote Sens. Environ.* **2020**, *242*, 111758. [CrossRef]
61. Barros, P.P.d.S.; Fiorio, P.R.; Demattê, J.A.d.M.; Martins, J.A.; Montezano, Z.F.; Dias, F.L.F. Estimation of leaf nitrogen levels in sugarcane using hyperspectral models. *Cienc. Rural* **2022**, *52*. [CrossRef]
62. Martins, J.A.; Fiorio, P.R.; Silva, C.A.A.C.; Demattê, J.A.M.; Barros, P.P.d.S. Application of Vegetative Indices for Leaf Nitrogen Estimation in Sugarcane Using Hyperspectral Data. *Sugar Tech* **2023**, *26*, 160–170. [CrossRef]
63. Naik, B.B.; Naveen, H.R.; Sreenivas, G.; Choudary, K.K.; Devkumar, D.; Adinarayana, J. Identification of Water and Nitrogen Stress Indicative Spectral Bands Using Hyperspectral Remote Sensing in Maize During Post-Monsoon Season. *J. Indian Soc. Remote Sens.* **2020**, *48*, 1787–1795. [CrossRef]
64. Tian, Y.; Yao, X.; Yang, J.; Cao, W.; Zhu, Y. Extracting Red Edge Position Parameters from Ground-and Space-Based Hyperspectral Data for Estimation of Canopy Leaf Nitrogen Concentration in Rice. *Plant Prod. Sci.* **2011**, *14*, 270–281. [CrossRef]
65. Cho, M.A.; Skidmore, A.K. A new technique for extracting the red edge position from hyperspectral data: The linear extrapolation method. *Remote Sens. Environ.* **2006**, *101*, 181–193. [CrossRef]
66. Ferwerda, J.G.; Skidmore, A.K. Can nutrient status of four woody plant species be predicted using field spectrometry? *ISPRS J. Photogramm. Remote Sens.* **2007**, *62*, 406–414. [CrossRef]
67. Sun, Y.; Qin, Q.; Ren, H.; Zhang, T.; Chen, S. Red-Edge Band Vegetation Indices for Leaf Area Index Estimation from Sentinel-2/MSI Imagery. *IEEE Trans. Geosci. Remote Sens.* **2020**, *58*, 826–840. [CrossRef]
68. Mu, X.; Chen, Y. The physiological response of photosynthesis to nitrogen deficiency. *Plant Physiol. Biochem.* **2021**, *158*, 76–82. [CrossRef] [PubMed]
69. Liang, L.; Di, L.; Huang, T.; Wang, J.; Lin, L.; Wang, L.; Yang, M. Estimation of leaf nitrogen content in wheat using new hyperspectral indices and a random forest regression algorithm. *Remote Sens.* **2018**, *10*, 1940. [CrossRef]
70. Peng, Y.; Zhu, X.; Xiong, J.; Yu, R.; Liu, T.; Jiang, Y.; Yang, G. Estimation of Nitrogen Content on Apple Tree Canopy through Red-Edge Parameters from Fractional-Order Differential Operators using Hyperspectral Reflectance. *J. Indian Soc. Remote Sens.* **2021**, *49*, 377–392. [CrossRef]
71. Zhao, B.; Duan, A.; Ata-Ul-Karim, S.T.; Liu, Z.; Chen, Z.; Gong, Z.; Zhang, J.; Xiao, J.; Liu, Z.; Qin, A.; et al. Exploring new spectral bands and vegetation indices for estimating nitrogen nutrition index of summer maize. *Eur. J. Agron.* **2018**, *93*, 113–125. [CrossRef]
72. Gitelson, A.A.; Zur, Y.; Chivkunova, O.B.; Merzlyak, M.N. Assessing Carotenoid Content in Plant Leaves with Reflectance Spectroscopy¶. *Photochem. Photobiol.* **2007**, *75*, 272–281. [CrossRef]
73. Liu, L.; Peng, Z.; Zhang, B.; Wei, Z.; Han, N.; Lin, S.; Chen, H.; Cai, J. Canopy nitrogen concentration monitoring techniques of summer corn based on canopy spectral information. *Sensors* **2019**, *19*, 4123. [CrossRef]
74. Li, L.; Lu, J.; Wang, S.; Ma, Y.; Wei, Q.; Li, X.; Cong, R.; Ren, T. Methods for estimating leaf nitrogen concentration of winter oilseed rape (*Brassica napus* L.) using in situ leaf spectroscopy. *Ind. Crops Prod.* **2016**, *91*, 194–204. [CrossRef]
75. Gates, D.M.; Keegan, H.J.; Schleter, J.C.; Weidner, V.R. Spectral Properties of Plants. *Appl. Opt.* **1965**, *4*, 11–20. [CrossRef]
76. Hussain, A.; Sahoo, R.N.; Kumar, D.; Pradhan, S. Relationship of Hyperspectral Reflectance Indices with Leaf N and P Concentration, Dry Matter Accumulation and Grain Yield of Wheat. *J. Indian Soc. Remote Sens.* **2017**, *45*, 773–784. [CrossRef]
77. Li, F.; Miao, Y.; Hennig, S.D.; Gnyp, M.L.; Chen, X.; Jia, L.; Bareth, G. Evaluating hyperspectral vegetation indices for estimating nitrogen concentration of winter wheat at different growth stages. *Precis. Agric.* **2010**, *11*, 335–357. [CrossRef]
78. Fang, M.; Ju, W.; Zhan, W.; Cheng, T.; Qiu, F.; Wang, J. A new spectral similarity water index for the estimation of leaf water content from hyperspectral data of leaves. *Remote Sens. Environ.* **2017**, *196*, 13–27. [CrossRef]
79. De Jong, S.M.; Addink, E.A.; Doelman, J.C. Detecting leaf-water content in Mediterranean trees using high-resolution spectrometry. *Int. J. Appl. Earth Obs. Geoinf.* **2014**, *27*, 128–136. [CrossRef]
80. Rodríguez-Pérez, J.R.; Ordóñez, C.; González-Fernández, A.B.; Sanz-Ablanedo, E.; Valenciano, J.B.; Marcelo, V. Leaf water content estimation by functional linear regression of field spectroscopy data. *Biosyst. Eng.* **2018**, *165*, 36–46. [CrossRef]
81. Fan, L.; Zhao, J.; Xu, X.; Liang, D.; Yang, G.; Feng, H.; Yang, H.; Wang, Y.; Chen, G.; Wei, P. Hyperspectral-based estimation of leaf nitrogen content in corn using optimal selection of multiple spectral variables. *Sensors* **2019**, *19*, 2898. [CrossRef]

82. García-Lara, S.; Serna-Saldivar, S.O. Corn History and Culture. In *Corn: Chemistry and Technology*, 3rd ed.; Woodhead Publishing: Duxford, UK, 2019; pp. 1–18. [CrossRef]
83. Repke, R.; Cruz, S.; Silva, C.; Figueiredo, P.; Bicudo, S. Eficiência da Azospirillum brasilense Combinada com Doses de Nitrogênio no Desenvolvimento de Plantas de Milho. *Rev. Bras. Milho Sorgo* **2013**, *12*, 214–226. [CrossRef]
84. Preza-Fontes, G.; Nafziger, E.D.; Christianson, L.E.; Pittelkow, C.M. Relationship of in-season soil nitrogen concentration with corn yield and potential nitrogen losses. *Soil Sci. Soc. Am. J.* **2020**, *84*, 1296–1306. [CrossRef]
85. Mahajan, G.R.; Das, B.; Murgaokar, D.; Herrmann, I.; Berger, K.; Sahoo, R.N.; Patel, K.; Desai, A.; Morajkar, S.; Kulkarni, R.M. Monitoring the Foliar Nutrients Status of Mango Using Spectroscopy-Based Spectral Indices and PLSR-Combined Machine Learning Models. *Remote Sens.* **2021**, *13*, 641. [CrossRef]
86. Yang, H.; Yin, H.; Li, F.; Hu, Y.; Yu, K. Machine learning models fed with optimized spectral indices to advance crop nitrogen monitoring. *Field Crops Res.* **2023**, *293*, 108844. [CrossRef]
87. Peng, Y.; Zhang, M.; Xu, Z.; Yang, T.; Su, Y.; Zhou, T.; Wang, H.; Wang, Y.; Lin, Y. Estimation of leaf nutrition status in degraded vegetation based on field survey and hyperspectral data. *Sci. Rep.* **2020**, *10*, 4361. [CrossRef] [PubMed]
88. Xia, T.; Miao, Y.; Wu, D.; Shao, H.; Khosla, R.; Mi, G. Active Optical Sensing of Spring Maize for In-Season Diagnosis of Nitrogen Status Based on Nitrogen Nutrition Index. *Remote Sens.* **2016**, *8*, 605. [CrossRef]
89. Chemura, A.; Mutanga, O.; Odindi, J.; Kutywayo, D.; Chemura, A.; Mutanga, O.; Odindi, J.; Kutywayo, D.; Chemura, A.; Mutanga, O.; et al. Mapping spatial variability of foliar nitrogen in coffee (*Coffea arabica* L.) plantations with multispectral Sentinel-2 MSI data. *ISPRS J. Photogramm. Remote Sens.* **2018**, *138*, 1–11. [CrossRef]
90. Shiratsuchi, L.; Ferguson, R.; Shanahan, J.; Adamchuk, V.; Rundquist, D.; Marx, D.; Slater, G. Water and Nitrogen Effects on Active Canopy Sensor Vegetation Indices. *Agron. J.* **2011**, *103*, 1815–1826. [CrossRef]
91. Azadnia, R.; Rajabipour, A.; Jamshidi, B.; Omid, M. New approach for rapid estimation of leaf nitrogen, phosphorus, and potassium contents in apple-trees using Vis/NIR spectroscopy based on wavelength selection coupled with machine learning. *Comput. Electron. Agric.* **2023**, *207*, 107746. [CrossRef]
92. Hatfield, J.L.; Prueger, J.H. Value of Using Different Vegetative Indices to Quantify Agricultural Crop Characteristics at Different Growth Stages under Varying Management Practices. *Remote Sens.* **2010**, *2*, 562–578. [CrossRef]
93. Gnyp, M.L.; Miao, Y.; Yuan, F.; Ustin, S.L.; Yu, K.; Yao, Y.; Huang, S.; Bareth, G. Hyperspectral canopy sensing of paddy rice aboveground biomass at different growth stages. *Field Crops Res.* **2014**, *155*, 42–55. [CrossRef]
94. Xue, J.; Su, B. Significant Remote Sensing Vegetation Indices: A Review of Developments and Applications. *J. Sens.* **2017**, *2017*, 1353691. [CrossRef]
95. Osco, L.P.; Junior, J.M.; Ramos, A.P.M.; Furuya, D.E.G.; Santana, D.C.; Teodoro, L.P.R.; Gonçalves, W.N.; Baio, F.H.R.; Pistori, H.; Junior, C.A.d.S.; et al. Leaf Nitrogen Concentration and Plant Height Prediction for Maize Using UAV-Based Multispectral Imagery and Machine Learning Techniques. *Remote Sens.* **2020**, *12*, 3237. [CrossRef]
96. Liu, N.; Xing, Z.; Zhao, R.; Qiao, L.; Li, M.; Liu, G.; Sun, H. Analysis of Chlorophyll Concentration in Potato Crop by Coupling Continuous Wavelet Transform and Spectral Variable Optimization. *Remote Sens.* **2020**, *12*, 2826. [CrossRef]
97. Wen, P.-F.; He, J.; Ning, F.; Wang, R.; Zhang, Y.-H.; Li, J. Estimating leaf nitrogen concentration considering unsynchronized maize growth stages with canopy hyperspectral technique. *Ecol. Indic.* **2019**, *107*, 105590. [CrossRef]
98. Liu, T.; Ren, T.; White, P.J.; Cong, R.; Lu, J. Storage nitrogen co-ordinates leaf expansion and photosynthetic capacity in winter oilseed rape. *J. Exp. Bot.* **2018**, *69*, 2995–3007. [CrossRef] [PubMed]
99. Fu, Y.; Yang, G.; Pu, R.; Li, Z.; Li, H.; Xu, X.; Song, X.; Yang, X.; Zhao, C. An overview of crop nitrogen status assessment using hyperspectral remote sensing: Current status and perspectives. *Eur. J. Agron.* **2021**, *124*, 126241. [CrossRef]
100. Wadoux, A.M.-C.; Heuvelink, G.B.; de Bruin, S.; Brus, D.J. Spatial cross-validation is not the right way to evaluate map accuracy. *Ecol. Model.* **2021**, *457*, 109692. [CrossRef]
101. King, R.D.; Orhobor, O.I.; Taylor, C.C. Cross-validation is safe to use. *Nat. Mach. Intell.* **2021**, *3*, 276. [CrossRef]